Retrievals of precipitable water vapor using star photometry: Assessment with Raman lidar and link to sun photometry

D. Pérez-Ramírez,[1,2] F. Navas-Guzmán,[1,2] H. Lyamani,[1,2] J. Fernández-Gálvez,[1,2] F. J. Olmo,[1,2] and L. Alados-Arboledas[1,2]

Received 22 June 2011; revised 20 December 2011; accepted 27 December 2011; published 1 March 2012.

[1] This work deals with the applicability of a star photometer to retrieve precipitable water vapor (*W*) at nighttime by means of direct irradiance from stars using a 940 nm narrowband filter. Retrievals are assessed with simultaneous data from a Raman lidar system and linked with daytime values from a sun photometer using measurements taken from March to May 2007 at an urban site. Calibration of both the star and sun photometers was performed by the Modified Astronomical Langley Method. The retrieval of *W* from photometers is based on a look up table using a simplified expression for the water vapor transmittance and the relative optical water vapor air mass. This methodology presents a systematic uncertainty in *W* below 3% and 6% for sun and star photometry, respectively. Retrievals of *W* from star photometry were 9% above those obtained from the Raman lidar technique, but with a great agreement in the temporal evolution from both instruments. The link of daytime and nighttime values of *W* using sun and star photometers for a more extended database showed a smooth continuity between consecutive periods.

Citation: Pérez-Ramírez, D., F. Navas-Guzmán, H. Lyamani, J. Fernández-Gálvez, F. J. Olmo, and L. Alados-Arboledas (2012), Retrievals of precipitable water vapor using star photometry: Assessment with Raman lidar and link to sun photometry, *J. Geophys. Res.*, *117*, D05202, doi:10.1029/2011JD016450.

1. Introduction

[2] Water vapor is one of the most important constituents in the Earth's atmosphere since it plays a key role in the global radiation budget and atmospheric energy transport mechanisms, as well as photochemical processes. Moreover, it is the most important gaseous source of infrared opacity in the atmosphere [*Trenberth et al.*, 2007], accounting for about 60% of the natural greenhouse effect for clear skies [*Kiehl and Trenberth*, 1997], and providing the largest positive feedback in model projections of climate change [*Held and Soden*, 2000]. In relation to radiative forcing, water vapor contributes directly to infrared radiation absorption emitted by the Earth's surface and the atmosphere [*Gerding et al.*, 2004]. It also contributes indirectly by means of microphysical processes leading to the formation and development of clouds, and further affects the size, shape and chemical composition of aerosols [*Reichardt et al.*, 1996], modifying their role in the radiative forcing [*De Tomasi and Perrone*, 2003]. Therefore, accurate estimates of water vapor are needed for meteorological and climatic purposes, including weather forecast and energy budget studies.

[3] Precipitable water vapor (*W*) is defined as the integrated amount of water vapor in the vertical column from the ground up to the top of the atmosphere. To study its spatial and temporal variability on daily and seasonal scales [*Trenberth et al.*, 2007], a wide variety of techniques have been developed. Global measurements of water vapor can be assessed from satellite platforms, such as the Moderate Resolution Imaging Spectroradiometer (MODIS [*Kaufman et al.*, 1997]) on NASA Aqua and Terra, the Atmospheric Infrared Sounder (AIRS [*Aumann et al.*, 2003]) on Aqua, and the Tropospheric Emission Spectrometer (TES [*Beer*, 2006]) on NASA Aura. However, satellite retrievals of *W* present large errors due to uncertainties in surface reflectivity (less reliable over land than over oceans), and has low temporal resolution. To address these limitations a wide range of ground measurements based on networks of observational stations are available worldwide, including radiosondes, sun photometers, lidar systems, microwave radiometers and global positioning system (GPS) receivers [*Alexandrov et al.*, 2009]. Nevertheless, from both a logistical and an economic point of view, it is rarely possible to obtain direct measurements of *W* at a large number of locations and with fine temporal resolution. Moreover, the knowledge of the interaction between spatial and temporal scales of processes is fundamental to understanding the behavior of the entire atmosphere.

[4] At coarse temporal and spatial resolution, the classic balloon-borne radiosonde remains the reference method for monitoring *W*, providing detailed profile information of water vapor content, but usually available only twice a day for selected sites. The *W* estimates from radiosondes also present some errors such as the overestimation of moisture after freezing and a subsequent latent heat release, the different time lags between dry and wet bulb temperature

[1]Centro Andaluz de Medio Ambiente, Universidad de Granada, Granada, Spain.
[2]Departamento de Física Aplicada, Universidad de Granada, Granada, Spain.

0148-0227/12/2011JD016450

measurements, and the absence of sampling at higher atmospheric layers [*Bruegge et al.*, 1992; *Campmany et al.*, 2010]. In this sense, *Bruegge et al.* [1992] estimated a relative error around 16% in the retrieval of W by radiosonde data. On the other hand, Raman lidar technique represents a powerful remote sensing tool to determine W through water vapor mixing ratio profiles obtained from the ratio of backscattered signals corresponding to water vapor and nitrogen [*Whiteman*, 2003]. However, due to low signal-to-noise ratio the majority of the Raman lidars only work at nighttime [*Goldsmith et al.*, 1998; *Whiteman et al.*, 2006]. This technique further requires calibration against radiosonde data, and the high cost and maintenance of Raman lidar systems limit their spatial and temporal resolution. Another alternative is ground-based microwave radiometry, which allows continuous estimates of W for nearly all weather conditions by measuring atmospheric emission at different frequencies in the microwave region [*Westwater*, 1978; *Rose et al.*, 2005; *Cimini et al.*, 2006]. Also, the GPS technique is able to provide continuous estimates of W over large number of locations through the GPS signal wet delay [*Bevis et al.*, 1992].

[5] Sun photometry has been increasingly used to obtain atmospheric extinction measurements in the visible and near infrared wavelengths. Aerosol optical depth and atmospheric columnar concentrations of gases such as ozone and water vapor can be derived from these measurements. The Aerosol Robotic Network (AERONET, http://aeronet.gsfc.nasa.gov/) [*Holben et al.*, 1998], provide W data worldwide during daytime and cloudless conditions with an uncertainty around 12% [*Holben et al.*, 1998].

[6] The aim of this work is to obtain nighttime data of W from star photometry measurements in a narrowband channel centered at 940 nm. The use of star photometry to retrieve W was first proposed by *Leiterer et al.* [1998] using the *Golubitsky and Moskalenko* [1968] water vapor transmittance and the two-star method. However, under non steady and inhomogeneous atmosphere, the two-star method is not reliable [*Pérez-Ramírez et al.*, 2011] and a methodology based on one-star measurements is used for accurate estimates of W.

[7] This paper is structured as follows: section 2 presents a short overview of the experimental site and the instruments used. Section 3 describes water vapor transmittance estimates from star and sun photometers measurements, and the subsequent retrieval of W from a look up table. Calibration procedures are given in section 4. Section 5 analyses the uncertainties associated with the retrieval of W from a look up table. Section 6 compares W data from star photometry and Raman lidar, including the daytime and nighttime evolution and continuity of W. Finally, section 7 summarizes the main conclusions.

2. Instrumentation and Experimental Site

[8] A star photometer (EXCALIBUR, iTec Astronómica S.L., Spain) was used to measure direct irradiance from stars. The incident light from a selected star is collected by a telescope (CELESTRON CGE 1100, United States) based on a Schmidt-Cassegrain optical system. The starlight passes through a filter wheel with six narrowband filters at 380, 436, 500, 670, 880 and 1020 nm for aerosol characterization, and an additional filter at 940 nm is used to retrieve W. These filters have Full Width at Half Maximum (FWHM) between 7.7 and 11.2 nm; particularly 11.2 nm for the 940 nm filter. The detector consists of a CCD camera (model SBIG ST8-XME, Santa Barbara, United States) and there is an additional wide-field camera attached to the telescope to assure correct pointing to a given star. The star photometer also incorporates software which is able to calculate the flat field, pointing and focusing to a selected star and calculate the background signal. Additional details can be found in the work of *Pérez-Ramírez et al.* [2008a, 2008b]. Calibration of the instrument was made at the German-Spanish Astronomical Center, "Calar Alto" (37.22°N, 2.55°W, 2168 m asl), a high mountain site fulfilling the requirements of low and stable aerosol load and W [*Sánchez et al.*, 2007].

[9] A sun photometer (CE-318-4, Cimel Electronique France) was used to acquire direct sun irradiance and sky radiance measurements. The direct sun irradiance measurements allow the retrieval of aerosol optical depth at six narrowband filters centered at 340, 380, 440, 670, 870, and 1020 nm (nominal wavelengths) and to obtain W by an additional filter centered at 936 nm. The typical FWHM values of the Cimel sun photometer are between 2 and 10 nm. This instrument follows the same calibration techniques and data quality protocol as those used in AERONET [*Holben et al.*, 1998; *Smirnov et al.*, 2000]. The calibration is performed in "Ahí de Cara," Sierra Nevada (37.12°N, 3.40°W, 2100 m asl) every 6 months, as this site presents low and stable aerosol load and W according to calibration requirements [*Alcántara et al.*, 2004; *Alados-Arboledas et al.*, 2008]. Further information on this instrument is to be found in the work of *Holben et al.* [1998].

[10] Lidar measurements were taken with a Raman lidar model LR331D400 (Raymetrics S.A., Greece). The Raman Lidar system is configured in a monostatic biaxial alignment pointing vertically to the zenith. The active source of the lidar system is a pulsed Nd:YAG laser with fundamental emission at 1064 nm, and additional emissions at 532 and 355 nm by using second and third harmonic generators. The repetition rate of the laser is 10 Hz. Output energies are 110, 65 and 60 mJ at 1064, 532 and 355 nm, respectively. The receiving system consists of a 0.4 m diameter Cassegrain telescope and a wavelength separation unit with dichroic mirrors, interferential filters and a polarization cube. Detection is carried out in seven channels corresponding to elastic wavelengths at 1064, 532p (parallel-polarized), 532s (perpendicular-polarized) and 355 nm, and 387 (nitrogen Raman-shifted signal from 355 nm), 408 nm (water vapor Raman-shifted signal from 355 nm) and 607 nm (nitrogen Raman shifted signal from 532 nm). Additional details can be found in the work of *Guerrero-Rascado et al.* [2008a]. This instrument operates in the framework of the European Aerosol Research Lidar Network (EARLINET, see http://www.earlinet.org/) [*Bösenberg et al.*, 2001] with regular measurements at nighttime twice a week as well as simultaneous measurements with CALIPSO satellite (see http://www-calipso.larc.nasa.gov/) overpasses [*Pappalardo et al.*, 2009].

[11] The instruments are deployed in the radiometric station of the University of Granada, located on the rooftop of the Andalusian Centre for Environmental Research (37.16°N, 3.60°W, 680 m asl). Granada is a medium-sized city placed in a natural basin surrounded by mountains and characterized by near-continental conditions with large seasonal

temperature differences (cool winters and hot summers). Most rainfall occurs during spring and winter time. The study area is about 200 km from the African continent and approximately 50 km away from the western Mediterranean basin. Due to its location in the Iberian Peninsula, the study area is affected by air masses coming from the Atlantic Ocean, the European and African continents and less frequently from the Mediterranean Sea [*Alados-Arboledas et al.*, 2003; *Lyamani et al.*, 2010]. The differences in temperature and relative humidity between these air masses induce remarkable changes in W throughout the year.

3. Methodology

[12] Both sun and star photometer measurements allow the retrieval of atmospheric transmittance for a window channel using the well known Beer-Bouguer-Lambert law. However, in the near infrared spectrum there is a strong wavelength-dependence absorption by water vapor. Around 940 nm there are a large number of randomly distributed spectral lines and the photometer response $V(940)$ at medium Earth-Sun distance is given by the following expression [*Bruegge et al.*, 1992; *Halthore et al.*, 1997]:

$$V(940) = V_0(940)\exp(-m_r\delta_{atm}(940))T_w(940), \quad (1)$$

where $V_0(940)$ is the calibration constant (signal that the instrument would measure out of the atmosphere), $\delta_{atm}(940)$ is the total atmospheric optical depth, $T_w(940)$ is the water vapor transmittance and m_r is the relative optical air mass given by *Kasten and Young* [1989]:

$$m_r = (\cos\theta + 0.15(93.885 - \theta)^{-1.253})^{-1}, \quad (2)$$

where θ is the solar/star zenith angle. The transmittance due to molecular scattering is computed using the Rayleigh expression and the very weak ozone absorption at 940 nm is computed according to *Gueymard* [2001]. The aerosol optical depth at 940 nm is obtained from a linear interpolation using the values at 880 and 1020 nm [*Halthore et al.*, 1997].

[13] In sun-photometry, a simplified relationship between $T_w(940)$ and W is widely used [*Halthore et al.*, 1997; *Holben et al.*, 1998; *Alexandrov et al.*, 2009]; this expression is given by

$$T_w(940) = \exp(-a(m_w W)^b), \quad (3)$$

where m_w is the relative optical water vapor air mass given by [*Gueymard*, 2001]

$$m_w = \left(\cos\theta + 0.311141\theta^{0.1}(92.4710 - \theta)^{-1.3814}\right)^{-1}. \quad (4)$$

[14] From equation (3), 'a' and 'b' are two unknown coefficients that depend on the central wavelength position, width and shape of the photometer filter function, as well as the atmospheric pressure-temperature lapse rate and the vertical distribution of water vapor [*Halthore et al.*, 1997; *Alexandrov et al.*, 2009]. Using MODTRAN3 radiative transfer code (http://modtran.org/), simulations made by *Halthore et al.* [1997] showed that these coefficients are approximately constant for midlatitudes (winter and summer) and tropical standard atmospheres using narrowband filters (FWHM below 10 nm) centered at 940.0 nm. Sun- and star-photometers filters have central wavelengths at 936.0 and 940.0, respectively, with FWHM of 10.0 and 11.23 nm. Therefore, differences in coefficients "a" and "b" are expected for the different filters.

[15] To avoid the dependence of $T_w(940)$ with the atmospheric temperature and humidity profiles, *Gueymard* [2001] proposed an expression obtained from MODTRAN simulated water vapor transmittances for a wide variety of atmospheric conditions:

$$T_w(\lambda) = \exp\left(-\left[(m_w W)^{1.05} f_w^n B_w A_{w,\lambda}\right]^c\right), \quad (5)$$

where $A_{w,\lambda}$ is the spectral absorption coefficient that together with coefficients f_w, n, c and B_w are obtained as an average from those computed for midlatitudes (winter and summer) and tropical standard atmospheres and depend on m_w and W. Particularly, the coefficient f_w is also related to the ratio p/p_0, where p is the atmospheric pressure and p_0 is the atmospheric pressure at sea level. Therefore, equation (5) is representative for a wide range of atmospheric conditions and used in SMARTS2 radiative transfer code for estimating $T_w(\lambda)$ in the near infrared [*Gueymard*, 2001]. The main disadvantages of this expression are that neither the calibration constant nor the analytical retrieval of W are permitted. Therefore, the use of a look up table to obtain W from $T_w(\lambda)$ and m_w is proposed. Values of m_w ranging from 1 to 8 at 0.01 intervals and W from 0.01 to 7 cm at 0.01 cm intervals are used in equation (5), with pressure given by a standard atmosphere, to compute the look up table. With the instrument calibrated, $T_w(\lambda)$ is obtained from the radiance measurements using equation (1) and m_w is computed from the zenith angle.

4. Calibration

4.1. Modified Langley Method and Modified Astronomical Langley Method

[16] The Modified Langley Method (MLM) is widely used in the literature for sun photometer calibration [*Halthore et al.*, 1997] but it requires low and stable W, which rarely occurs except in high mountain sites [*Schmid et al.*, 1998; *Alexandrov et al.*, 2009]. It is based on using equation (3) and applying natural logarithms to equation (1),

$$\ln V(940) + m_r\delta_{atm}(940) = \ln V_0(940) - a(m_w W)^b, \quad (6)$$

from where measurements of $V(940)$ over a wide range of m_w and plotting ($\ln V(940) + m_r\ \delta_{atm}(940)$) versus m_w^b, allow calculation of the calibration constant $V_0(940)$ and W from the ordinate intercept and the slope through a least squares fit.

[17] Sun and star photometer measurements are affected by atmospheric turbulence, which is responsible for signal fluctuations, more critical in star photometry due to the low signal-to-noise ratio. Furthermore, due to technical specifications of the star photometer, few measurements are acquired at large m_w [*Pérez-Ramírez et al.*, 2011] and are poorly representative for the MLM fit. Therefore, a Modified Astronomical Langley Method (MALM) calibration is proposed based on the same equation but divided by m_w^b,

$$\frac{\ln V(940) + m_r\delta_{atm}(940)}{m_w^b} = \frac{\ln V_0(940)}{m_w^b} - aW^b. \quad (7)$$

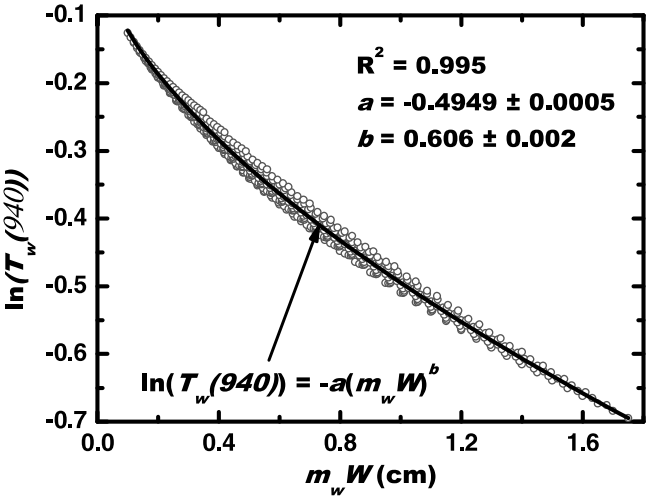

Figure 1. Computed values of ln $T_w(\lambda)$ versus m_wW using equation (5): m_w from 1 to 3.5 (step 0.01) and W from 0.1 to 0.5 cm (step 0.01 cm). The solid curve corresponds to the power fit indicated by the equation.

[18] In this case, the calibration constant $V_0(940)$ is obtained from the slope of the least squares fit $(\ln V(940) + m_r\delta(940))/m_w^b$ versus $1/m_w^b$. Physically, the change of variable in equation (7) refers to equivalent measurements at the zenith, being the apparent extraterrestrial value $\ln V'_0(940\text{ nm}) = \ln V_0(940\text{ nm})/m_w^b$ related to the different paths of the atmospheric radiation.

4.2. Raman Lidar Calibration

[19] Deriving water vapor mixing ratio, $q(z)$, with a Raman lidar system involves the detection of the backscattered signals from two vibration bands, one corresponding to the water vapor $P(\lambda H_2O, z)$ (407 nm) and the other to a reference gas, in this case nitrogen, $P(\lambda N_2, z)$ (387 nm). The ratio of these two signals reads as follows [*Whiteman*, 2003]:

$$\frac{P(\lambda_{H_2O}, z)}{P(\lambda_{N_2}, z)} = C\,q(z)\exp\left\{-\int_0^{\zeta}(\alpha(\lambda_{N_2}, \zeta) - \alpha(\lambda_{H_2O}, \zeta))d\zeta\right\}, \tag{8}$$

where α_{N2} and α_{H2O} are the extinction coefficients of nitrogen and water vapor, respectively, and C is a calibration constant taking into account the fractional volume of nitrogen in the atmosphere, the ratio of molecular masses, the range-independent calibration constants for the 387 and 408 nm channels and the independent Raman backscattered cross sections of nitrogen and water vapor. Assuming identical overlap factor for both signals it is possible to obtain measurements at lower altitudes [*Whiteman et al.*, 1992; *Goldsmith et al.*, 1998]. As the lidar system uses a biaxial configuration, with no overlap in the first few meters between the field of view of the telescope and the laser beam, 150 m above the lidar system was considered appropriate for reliable water vapor measurements, leaving below unrealistic values close to the surface where the ratio between the two weak signals is responsible for large fluctuations in the measurements.

[20] The calibration constant was obtained during an experimental campaign at "El Arenosillo" (37.11°N, 6.73°W, 0 m asl) comparing $q(z)$ from this instrument with those derived from simultaneous radiosonde data using an altitude range between 1 and 2.5 km a.g.l. This range was selected in order to minimize the effect of sonde drift by wind and also because it represents the best agreement during calibration with reference radiosonde data [*Guerrero-Rascado et al.*, 2008b]. A similar altitude range has also been used by other authors [*Gerding et al.*, 2004]. The mean value together with the standard deviation obtained for C was 116.6 ± 1.3 g kg^{-1}. Using this calibration constant, q(z) profiles obtained by the lidar system were compared with those obtained by another six radiosondes launched during the calibration campaign, being the least squares error of 7.8% which is within the values reported in the literature [*Mattis et al.*, 2002]. Due to the low intensity of Raman signals, $P(\lambda_{H_2O}, z)$ and $P(\lambda_{N_2}, z)$ of our instrument are only retrieved at nighttime when the sky background radiance is low and steady enough.

4.3. Photometers Calibration

[21] From 18 December 2006 to 12 January 2007, a star photometer calibration campaign was carried out in "Calar Alto," with 12 nights fulfilling cloudless and stable atmospheric conditions. Photometers calibration require the use of equation (3) where coefficients 'a' and 'b' related to coefficients from equation (5) as $a = (f_w^n B_w A_w)^c$ and $b = 1.05c$. Moreover, assuming 'a' and 'b' approximately constant within the short intervals of W and m_w values in a high mountain site, then both coefficients are obtained through a power fit ln $T_w(940) = -aX^b$, where $X = m_wW$ and computing $T_w(940)$ from equation (5). Figure 1 shows the power fit for representative values during the calibration campaign: m_w from 1 to 3.0 (step 0.01) and W from 0.1 to 0.5 cm (step 0.01 cm). Thus an equivalent expression similar to equation (3) will be obtained. The pressure level at 2168 m a.s.l ("Calar Alto") and a standard atmosphere were used in the computation, obtaining $a = 0.4949 \pm 0.0005$ and $b = 0.606 \pm 0.002$. The relative difference between $T_w(940)$ from equation (3) and the one computed from equation (5) was 0.8 ± 0.5%, with a minimum relative difference of 0.003% and a maximum relative difference of 2.1%. Therefore, these values of coefficients 'a' and 'b' were used for star photometer calibration.

[22] Figures 2a and 2b show the MLM and the MALM calibration plots for the star DENEB on 7 January 2007, respectively. The uncertainties in the determination of $V_0(940)$ can arise from the finite FWHM of the filters, errors in m_r and m_w, as well as the variability of $\delta_{atm}(\lambda)$ and W during measurements [*Schmid and Wehrli*, 1995]. The main source of error is associated with $\delta_{atm}(940)$ which is close to 0.02, while errors for m_r, m_w and $V(940\text{ nm})$ are below 0.001 [*Pérez-Ramírez et al.*, 2011]. The calibration constant $V_0(940)$ using MLM was 106900 ± 1200 photon counts (linear determination coefficient, R^2, equals to 0.953), while $V_0(940)$ obtained from MALM was 106300 ± 700 photon counts ($R^2 = 1.000$). The difference in the calibration constants from both methods is within the experimental uncertainty, but the MALM provides a better linear correlation coefficient. As previously indicated, the MALM minimizes the effects of large m_w in the linear fit, allowing a calibration for m_w between 1 and 3, the usual operational range of the

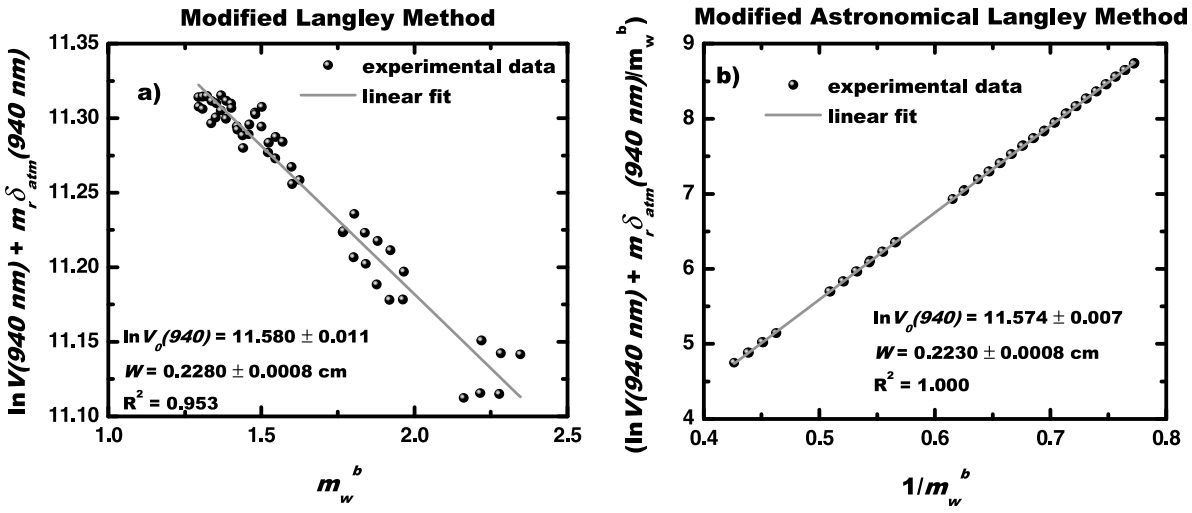

Figure 2. Calibration of the star DENEB on 7 January 2007 at Calar Alto Astronomical Center (2168 m asl) by (a) Modified Langley Method and (b) Modified Astronomical Langley Method. Experimental errors for m_r, m_w and V(940 nm) are negligible while error in δ_{atm}(940) is close to 0.02.

instrument [*Pérez-Ramírez et al.*, 2011]. Moreover, the MALM is less affected by atmospheric turbulence effects.

[23] The accuracy of the calibration constant determined by MLM and MALM was evaluated by checking its reproducibility. The star DENEB was also calibrated on 29 December 2006, obtaining V_0(940) values of 102000 ± 2000 and 106000 ± 2000 photon counts for MLM and MALM, respectively. The calibration constant was similar using MALM in the two different nights but not for MLM. Similar results were obtained with other stars; then, calibration constants from MALM were used in this work. Table 1 shows mean values of V_0(940) for at least two nights for each of the stars used during the calibration campaign at "Calar Alto." The average relative error in the calibration constant, $\Delta V_0(940)/V_0(940)$, including all stars was 0.015.

[24] The same calibration procedure was also used for the sun photometer in "Ahí de Cara," with W varying from 0.01 cm to 0.5 cm and m_w from 2 to 7. Coefficients obtained were $a = 0.44000 \pm 0.00014$ and $b = 0.5779 \pm 0.0005$, close to those from the star photometer. The slight difference in filter FWHM and the range of fitting values is responsible for these small discrepancies (<5%). The MALM provided a mean V_0(940) of 5100 photon counts for the sun photometer, with no significant changes from 2005 to 2008. The computed uncertainties in the calibration constant for the sun photometer was 0.01.

5. Error Analysis on the Retrieval of Precipitable Water Vapor

[25] For sun and star photometers the maximum error in the measured water vapor transmittance, $\Delta T_w(940)$, is given by

$$\Delta T_w(940) = T_w(940)\left|\frac{\Delta V(940)}{V(940)} + \frac{\Delta V_0(940)}{V_0(940)} + m_r\left(\frac{\Delta\delta_A(880) + \Delta\delta_A(1020)}{2}\right)\right|, \quad (9)$$

where ΔV(940) is the error associated with the measurement at 940 nm, ΔV_0(940) is the error associated with the calibration constant, and $\Delta\delta_A$(880) and $\Delta\delta_A$(1020) are the errors in aerosol optical depths at 880 and 1020 nm, respectively. For the filters used in the sun and star photometers, errors in aerosol optical depth, $\Delta\delta_A(\lambda)$ are close to $\Delta\delta_{atm}(\lambda)$, with negligible errors associated to molecular scattering and absorption by O_3 and NO_2 optical depths [*Reagan et al.*, 1986]; therefore equation (9) uses $\Delta\delta_A(\lambda)$ instead of $\Delta\delta_{atm}(\lambda)$. Additionally errors in m_r are negligible for $m_r < 6$ according to *Iqbal* [1983]. Particularly in this case, errors in aerosol optical depth at these wavelengths are close to 0.01 and the ratio $\Delta V(940)/V(940)$ is 1 order of magnitude lower than the average relative error in the calibration constants, $\Delta V_0(940)/V_0(940)$, evaluated as 0.015 [*Pérez-Ramírez et al.*, 2011]. Then for the star photometer, $\Delta T_w(940) \approx 0.03 T_w(940)$ for $m_r = 1$. Similarly, for the sun photometer, the ratio $\Delta V_0(940)/V_0(940)$ is approximately 0.01, $\Delta\delta_A(880)$ and $\Delta\delta_A(1020)$ are close to 0.01, and the

Table 1. Calibration Constants and Their Associated Relative Errors $\Delta V_0(940)/V_0(940)$ for the Stars Used During the Winter 2006/2007 Campaign Using the Modified Astronomical Langley Method[a]

Stars	V_0(940) Photon Counts
HR15	36,000 ± 600
MIRFAK	110,000 ± 2000
ALDEBARAN	803,000 ± 14,000
CAPELLA	623,000 ± 9000
SA040750	51,000 ± 800
CASTOR	76,000 ± 1000
PROCYON	342,000 ± 4000
POLLUX	278,000 ± 3000
REGULUS	75,000 ± 1400
DUBHE	172,000 ± 3000
HR7796	74,000 ± 1400
DENEB	106,000 ± 1500

[a]Values correspond to the mean of at least two nights of measurements for each star.

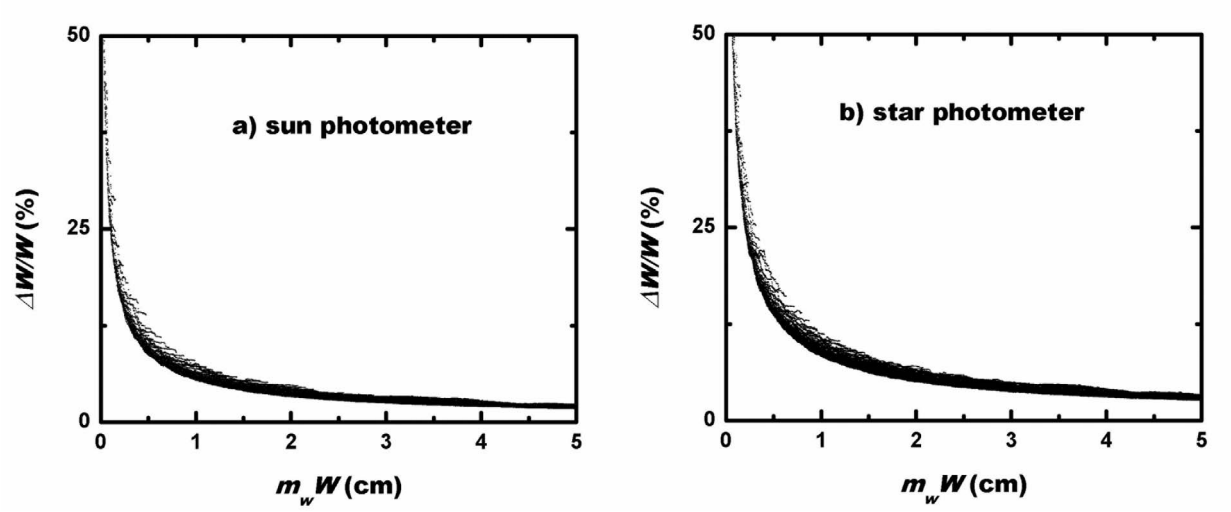

Figure 3. Relative differences of precipitable water vapor retrieved by a look up table as a function of the water vapor optical relative air mass multiplied by the precipitable water vapor for the (a) sun and (b) star photometer. Superposition of symbol is due to similar m_wW with different $\Delta W/W$ values.

ratio $\Delta V(940)/V(940)$ is also negligible [*Holben et al.*, 1998]. Therefore, $\Delta T_w(940) \approx 0.02 T_w(940)$ for $m_r = 1$.

[26] The error in W was evaluated by Monte Carlo techniques, assuming that uncertainties in $T_w(940)$ follows a Gaussian distribution centered at $T_w(940)$ and with a standard deviation of $\Delta T_w(940)$ (equation (9)). A set of randomly generated $T'_w(940)$ and their corresponding W' was computed by means of a look up table. By definition, the mean of W' is equal to W obtained from $T_w(940)$, and the standard deviation is associated with ΔW. This procedure was applied for W varying from 0.01 to 3 cm (step 0.01 cm) and m_w from 1 to 3 (step 0.01). The relative differences $\Delta W/W$ as a function of m_wW for sun and star photometers are shown in Figure 3. As can be observed, $\Delta W/W$ for the star photometer is larger than 25% for $m_wW < 0.2$ cm, decreasing to 3% for $m_wW > 5$ cm. Relative errors computed for the sun photometer follows the same pattern but with lower values; above 15% for $m_wW < 0.2$ cm decreasing to 2% for $m_wW > 5$ cm.

[27] A statistical analysis of W from March 2007 to June 2008 has revealed daytime W varying from 0.2 to 2.7 cm with a mean value for the entire period of 1.4 ± 0.5 cm, average m_w of 1.5, and therefore $\Delta W/W$ was close to 3% for the sun photometer. Similarly analysis for nighttime has showed that W varied from 0.2 to 3.0 cm, with a mean value for the entire period of 1.4 ± 0.5 cm, the average m_w of 1.25, and average $\Delta W/W$ was close to 6%.

[28] The error analysis just mentioned is associated with systematic errors due to uncertainties in the calibration constant. However, there are other errors that can be associated with the spectral database used and make discrepancies within the different techniques to retrieve W [*Alexandrov et al.*, 2009].

Table 2. Measurements Taken With the Lidar System Between March and May 2007

Dates	Hours (UTC)
8 Mar 2007	20:03–22:03
22 Mar 2007	01:00–02:00
17 Apr 2007	19:30–22:30
19 Apr 2007	21:45–22:45
30 Apr 2007	01:30–02:30 and 20:00–22:00
7 May 2007	20:00–22:00
8 May 2007	20:00–23:59
9 May 2007	00:00–04:00
10 May 2007	20:00–22:00
14 May 2007	20:00–22:00
16 May 2007	01:30–03:30
17 May 2007	20:00–22:00

6. Assessment With Raman Lidar and Link to Sun Photometry

[29] Sun and star photometers were measuring on a regular basis during the monitoring period even though only

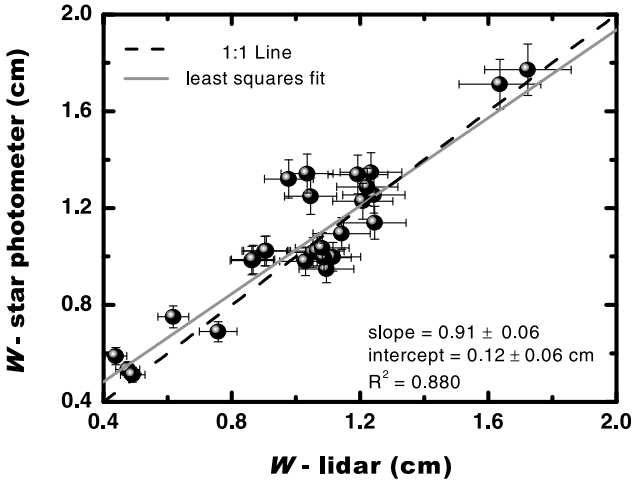

Figure 4. Comparison between precipitable water vapor retrieved by the lidar system and the star photometer from March 2007 to May 2007. Bars correspond to the experimental errors on measurements.

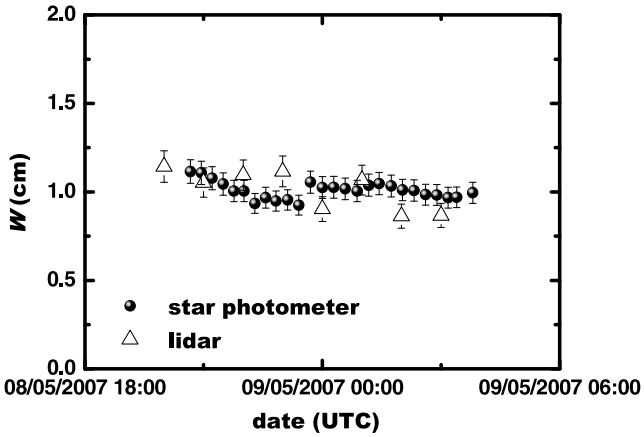

Figure 5. Precipitable water vapor retrieved during the one night from 8 to 9 May 2007 using both the star photometer and the lidar system. Bars correspond to the experimental errors on measurements.

cloudless data are actually used; nevertheless lidar measurements were only limited to operational protocols of the EARLINET network. Measurements taken by the lidar system during the study period are summarized in Table 2. Mean values of water vapor mixing ratio profiles were computed by averaging one hour of lidar measurements, then W is calculated by integrating $q(z)$ for the entire atmospheric profile. To address for the incomplete overlap for the first 150 m a.g.l., it is assumed a constant $q(z)$ from this level down to ground. Differences between the water vapor mixing ratio independently measured at ground level and that obtained at the lowest-altitude values from the lidar system were between 10 and 20%. Nevertheless, the W values computed assuming a constant mixing ratio for the first 150 m a.g.l. are 1.5% lower than the W obtained from a linear interpolation between the surface and the lowest-altitude value from the lidar system.

Table 3. Mean Daytime and Nighttime Values of Precipitable Water Vapor for a Selected Period From 9 to 12 May 2007[a]

	9 May 2007	10 May 2007	11 May 2007	12 May 2007
Day	1.25 ± 0.17	1.06 ± 0.08	1.03 ± 0.09	1.51 ± 0.11
Night	1.22 ± 0.04	1.03 ± 0.04	1.14 ± 0.03	1.38 ± 0.14

[a]Mean precipitable water vapor is in cm.

These values are within the uncertainty of the star photometer and lidar system.

[30] In total, there were 28 lidar measurements of W allowing direct comparison with values obtained from star photometry (Figure 4). The range of W values goes from 0.43 to 1.80 cm with a strong correlation between both instruments ($R^2 = 0.880$). The proximity of the data points to the 1:1 line as well as the slope (0.91 ± 0.06) and intercept (0.12 ± 0.06 cm) of the linear fit reflects the agreement between both instruments. In spite of the slope, star photometer data are only 3% lower on average than those from lidar due to the nonzero intercept. This bias between the instruments is lower than the systematic uncertainties associated with the methodology used for derived W from the star photometer (6% as indicated in section 5) and the uncertainty of the lidar system (6.5% as stated by *Whiteman et al.* [2006]). Furthermore, differences in the techniques must be taken into account. In this sense, retrievals of W during daytime using different techniques have been widely discussed in the literature, reporting uncertainties up to 15% between sun photometry and radiousonde data [*Halthore et al.*, 1997; *Schmid et al.*, 2001; *Campmany et al.*, 2010], and remarking systematic underestimation of microwave radiometer data over multifilter rotating shadowband radiometers [*Alexandrov et al.*, 2009].

[31] As can be observed from Figure 4, there is an agreement between both instruments for the entire range of W. Changes in W are directly related to air temperature; saturated vapor pressure rises with temperature and so it affects the

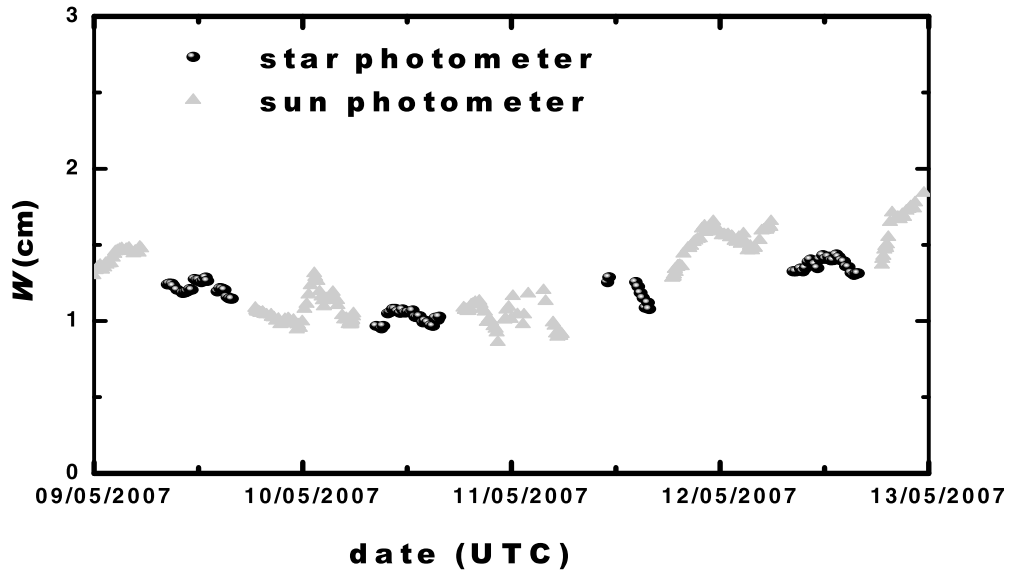

Figure 6. Daytime and nighttime precipitable water vapor from 9 May 2007 12:00 UTC to 13 May 2007 12:00 UTC combining sun and star photometers.

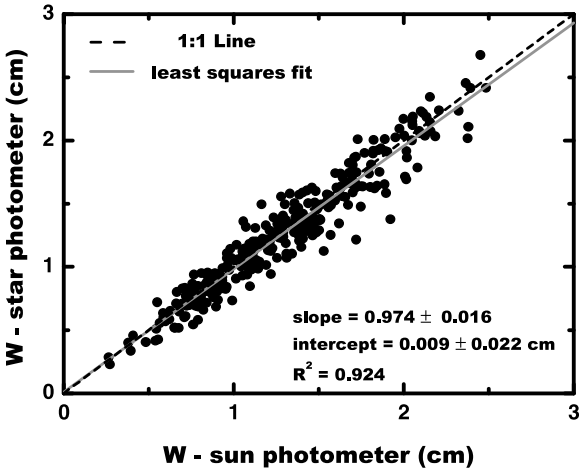

Figure 7. Comparison between precipitable water vapor for the last/first data at daytime retrieved by the sun photometer and the first/last data at nighttime retrieved by the star photometer. Mean values were computed within the 2 h interval at sunset and sunrise from March 2007 to June 2008.

amount of water vapor that can be stored without reaching saturation. In this case, the atmosphere was colder in March than in May, therefore W had usually lower values in March. Moreover, the night-to-night fluctuations of W can be associated with changes in the air masses reaching the site.

[32] Figure 5 shows a detailed analysis of W measurements for one night, 8 to 9 May 2007, as an example of results corresponding to fine time resolution. Data from both instruments agree and show a similar trend with a maximum difference in W close to 5%; the slight decrease in W through the night is evidenced for both instruments. For the star photometer, the mean value of W corresponding to this night was 1.01 ± 0.04 cm, with maximum and minimum values of 1.12 and 0.93 cm, respectively. The mean value obtained from the lidar system was 1.01 ± 0.11 cm, with maximum and minimum values of 1.14 and 0.86 cm, respectively. Air masses reaching the city of Granada were identified using 5 day backward trajectories computed by the HYSPLIT model (R. R. Draxler and G. D. Rolph, HYSPLIT - Hybrid Single-Particle Lagrangian Integrated Trajectory Model, 2003, http://ready.arl.noaa.gov/HYSPLIT.php) at 500, 1500 and 3500 m a.g.l. Particularly, on this night backward trajectories at all the altitudes were coming from the North Atlantic and the Iberian Peninsula, bringing warm air masses with considerable water vapor content.

[33] The combination of sun and star photometers is very useful for computing W at daytime and nighttime with high temporal resolution and low maintenance. In this sense, Figure 6 shows an example from 9 May 2007 12:00 UTC to 13 May 2007 12:00 UTC. During the night from 11 to 12 May 2007, thin cirrus clouds between 23:15 to 02:15 UTC reduced the number of available data. Daytime and nighttime mean values of W for these days are shown in Table 3. Changes in W between day-to-day and night-to-night show irregular patterns associated with the air masses passing over the site. The evolution of W throughout the entire day presented a smooth behavior, with changes due to the intrinsic variability of W.

[34] The continuity between daytime and nighttime measurements of W is evidenced comparing the last/first data obtained at daytime by the sun photometer and the first/last data obtained at nighttime by the star photometer. For this purpose, 2 h time intervals at both sunset and sunrise were used to compute the mean and standard deviation of W in each case. Figure 7 shows the least square fit of nighttime values versus those at daytime. Only data showing standard deviation below 0.05 cm were used in order to avoid scenarios with strong variability in W, resulting 297 pairs of data for an extended data set from March 2007 to June 2008.

[35] As indicated in Figure 7, there is a strong correlation between daytime and nighttime values ($R^2 = 0.924$). The slope (0.974 ± 0.016) is near to one and the intercept (0.009 ± 0.022 cm) close to zero. The correlation including only sunset values (145 data) reveals $R^2 = 0.906$ with 0.96 ± 0.03 slope and 0.02 ± 0.04 cm intercept, while at sunrise (152 data) reveals $R^2 = 0.945$ with 0.99 ± 0.02 slope and -0.009 ± 0.022 cm intercept.

7. Conclusions

[36] A variety of measurements using sun and star photometry as well as Raman lidar technique has been used to characterize atmospheric W during daytime and nighttime from March to May 2007 at an urban site. The applicability of a star photometer to retrieve W during nighttime using a 940 nm narrowband filter has been satisfactory tested. The retrieval of W from photometers is based on a look up table using $T_w(940)$ and m_w as inputs, where $T_w(940)$ is described by the general equation used in SMARTS2 radiative transfer code. Photometers calibration at 940 nm channel was performed at high mountain sites using the MALM, providing satisfactory correlation coefficients ($R > 0.999$) and reproducible results. Moreover, this type of calibration minimizes uncertainties caused by atmospheric turbulences and reduces the effect of the limited interval of water vapor air masses used in star photometry. A detailed analysis using Monte Carlo technique and error propagation on $T_w(940)$ revealed systematic relative errors for W below 3% and 6% for sun and star photometers, respectively.

[37] Retrievals of W from star photometry were on average 9% larger than those obtained from the Raman lidar technique. These differences have been associated with uncertainties in the calibration constants of the instruments. Moreover, there was a good agreement in the temporal evolution of W retrieved from both instruments and the analysis of sun and star photometer data within the 2 h around sunset and sunrise show a remarkable continuity between both instruments. Therefore, from this work, daytime and nighttime measurement combining sun and start photometers represent a great opportunity for continuous monitoring of W through the entire day, key for better understanding the role of water vapor in Earth's climate system.

[38] **Acknowledgments.** This work was supported by the Spanish Ministry of Science and Technology through projects CGL2008-01330-E/CLI (Spanish Lidar Network), CGL2010–18782 and CSD2007–00067; by the Andalusian Regional Government through projects P10-RNM-6299 and P08-RNM-3568; and by the EU ACTRIS project (EU INFRA-2010-1.1.16–262254). The authors would like to express their gratitude to the NASA Goddard Space Flight Center, NOAA Air Resources Laboratory and Naval Research Laboratory for the HYSPLIT model. We also thank

Calar Alto Astronomical Center for the facilities provided to calibrate the star photometer. We also express our gratitude to the anonymous referees for their suggestions to improve this work.

References

Alados-Arboledas, L., H. Lyamani, and F. J. Olmo (2003), Aerosol size properties at Armilla, Granada (Spain), *Q. J. R. Meteorol. Soc.*, *129*, 1395–1413, doi:10.1256/qj.01.207.

Alados-Arboledas, L., et al. (2008), Aerosol columnar properties retrieved from CIMEL radiometers during VELETA 2002, *Atmos. Environ.*, *42*, 2654–2667, doi:10.1016/j.atmosenv.2007.10.006.

Alcántara, A., F. J. Olmo, and L. Alados-Arboledas (2004), Langley calibrations of sunphotometer at Sierra Nevada, Granada, Spain, *Opt. Pura Apl.*, *37*, 3263–3269.

Alexandrov, M. D., B. Schmid, D. D. Turner, B. Cairns, V. Oinas, A. A. Lacis, S. I. Gutman, E. R. Westwater, A. Smirnov, and J. Eilers (2009), Columnar water vapor retrievals from multifilter rotating shadowband radiometer data, *J. Geophys. Res.*, *114*, D02306, doi:10.1029/2008JD010543.

Aumann, H. H., et al. (2003), AIRS/AMSU/HSB on the Aqua mission: Design, science objectives, data products, and processing system, *IEEE Trans. Geosci. Remote Sens.*, *41*, 253–264, doi:10.1109/TGRS.2002.808356.

Beer, R. (2006), TES on the Aura Mission: Scientific objectives, measurements, and analysis overview, *IEEE Trans. Geosci. Remote Sens.*, *44*, 1102–1105, doi:10.1109/TGRS.2005.863716.

Bevis, M., S. Businger, T. A. Herring, C. Rocken, R. A. Anthes, and R. H. Ware (1992), GPS meteorology: Remote sensing of atmospheric water vapor using the Global Positioning System, *J. Geophys. Res.*, *97*, 15,787–15,801, doi:10.1029/92JD01517.

Bösenberg, J., et al. (2001), EARLINET: A European aerosol research lidar network, laser remote sensing of the atmosphere, paper presented at 20th International Laser Radar Conference, Ec. Polytech., Vichy, France, 10–14 Jul.

Bruegge, C. J., J. E. Conel, J. S. Green, J. S. Margolis, R. G. Holm, and G. Toon (1992), Water vapor column abundance retrievals during FIFE, *J. Geophys. Res.*, *97*, 759–768, doi:10.1029/92JD01050.

Campmany, E., J. Bech, J. Rodríguez-Marcos, Y. Sola, and J. Lorente (2010), A comparison of total precipitable water measurements from radiosonde and sunphotometers, *Atmos. Res.*, *97*, 385–392, doi:10.1016/j.atmosres.2010.04.016.

Cimini, D., T. J. Hewison, L. Martin, J. Güldner, C. Gaffard, and F. S. Marzano (2006), Comparison of brightness temperatures observed from ground-based microwave radiometers during TUC, *Meteorol. Z.*, *15*, 19–25, doi:10.1127/0941-2948/2006/0096.

De Tomasi, F., and M. R. Perrone (2003), Lidar measurements of tropospheric water vapor and aerosol profiles over southeastern Italy, *J. Geophys. Res.*, *108*(D9), 4286, doi:10.1029/2002JD002781.

Gerding, M., C. Ritter, M. Müller, and R. Neuber (2004), Tropospheric water vapour soundings by lidar at high Arctic latitudes, *Atmos. Res.*, *71*, 289–302, doi:10.1016/j.atmosres.2004.07.002.

Goldsmith, J. E., F. H. Blair, S. E. Bisson, and D. D. Turner (1998), Turn-key Raman lidar for profiling atmospheric water vapor, clouds and aerosols, *Appl. Opt.*, *37*, 4979–4990, doi:10.1364/AO.37.004979.

Golubitsky, B. M., and N. I. Moskalenko (1968), Funkzii spektralnowo propuskanija *W* polosach parow H_2O i CO_2, *Izv. Akad. Nauk SSSR Fiz. Atmos. Okeana*, *4*, 346–359.

Guerrero-Rascado, J. L., B. Ruiz, and L. Alados-Arboledas (2008a), Multi-spectral lidar characterization of the vertical structure of Saharan dust aerosol over southern Spain, *Atmos. Environ.*, *42*, 2668–2681, doi:10.1016/j.atmosenv.2007.12.062.

Guerrero-Rascado, J. L., B. Ruiz, G. Gourdakis, G. Georgoussis, and L. Alados-Arboledas (2008b), One year of water vapour Raman lidar measurements at the Andalusian Centre for Environmental Studies (CEAMA), *Int. J. Remote Sens.*, *29*, 5437–5453, doi:10.1080/01431160802036433.

Gueymard, C. A. (2001), Parameterized transmittance model for direct beam and circumsolar spectral irradiance, *Sol. Energy*, *71*, 325–346, doi:10.1016/S0038-092X(01)00054-8.

Halthore, R. N., T. F. Eck, N. B. Holben, and B. L. Markham (1997), Sun photometric measurements of atmospheric water vapor, *J. Geophys. Res.*, *102*, 4343–4352, doi:10.1029/96JD03247.

Held, I. M., and B. J. Soden (2000), Water vapor feedback and global warming, *Annu. Rev. Energy Environ.*, *25*, 441–475, doi:10.1146/annurev.energy.25.1.441.

Holben, B. N., et al. (1998), AERONET—A Federated instrument network and data archive for aerosol characterization, *Remote Sens. Environ.*, *66*, 1–16, doi:10.1016/S0034-4257(98)00031-5.

Iqbal, M. (1983), *An Introduction to Solar Radiation*, 390 pp., Academic, Toronto, Ont., Canada.

Kasten, F., and A. T. Young (1989), Revised optical air mass table and approximation formula, *Appl. Opt.*, *28*, 4735–4738, doi:10.1364/AO.28.004735.

Kaufman, Y. J., D. Tanré, L. A. Remer, E. Vermote, A. Chu, and B. N. Holben (1997), Operational remote sensing of tropospheric aerosol over the land from EOS moderate resolution imaging spectroradiometer, *J. Geophys. Res.*, *102*, 17,051–17,067, doi:10.1029/96JD03988.

Kiehl, J. T., and K. E. Trenberth (1997), Earth's annual global mean energy budget, *Bull. Am. Meteorol. Soc.*, *78*, 197–208, doi:10.1175/1520-0477(1997)078<0197:EAGMEB>2.0.CO;2.

Leiterer, U., G. Alekseeva, V. Galking, H. Dier, J. Gülden, A. Naebert, T. Naebert, V. Novikov, H. Rentsch, and G. Sakunov (1998), Water vapour column content and optical depths measurements by a sun and star photometer, *Contrib. Atmos. Phys.*, *71*, 401–420.

Lyamani, H., F. J. Olmo, and L. Alados-Arboledas (2010), Physical and optical properties of aerosols over an urban location in Spain: Seasonal and diurnal variability, *Atmos. Chem. Phys.*, *10*, 239–254, doi:10.5194/acp-10-239-2010.

Mattis, I., A. Ansman, D. Althausen, V. Jaenisch, U. Wandinger, D. Mueller, Y. F. Arshinov, S. M. Bobrovnikov, and I. B. Serikov (2002), Relative-humidity profiling in the troposphere with a Raman lidar, *Appl. Opt.*, *41*, 6451–6462, doi:10.1364/AO.41.006451.

Pappalardo, G., et al. (2009), EARLINET correlative measurements for CALIPSO: First intercomparison, *J. Geophys. Res.*, *115*, D00H19, doi:10.1029/2009JD012147.

Pérez-Ramírez, D., J. Aceituno, B. Ruiz, F. J. Olmo, and L. Alados-Arboledas (2008a), Development and calibration of a star photometer to measure the aerosol optical depth: Smoke observations at a high mountain site, *Atmos. Environ.*, *42*, 2739–2745, doi:10.1016/j.atmosenv.2007.06.009.

Pérez-Ramírez, D., B. Ruiz, J. Aceituno, F. J. Olmo, and L. Alados-Arboledas (2008b), Application of sun/star photometry to derive the aerosol optical depth, *Int. J. Remote Sens.*, *29*, 5113–5132, doi:10.1080/01431160802036425.

Pérez-Ramírez, D., H. Lyamani, F. J. Olmo, and L. Alados-Arboledas (2011), Improvements on star photometry for aerosol characterization, *J. Aerosol Sci.*, *42*, 737–745, doi:10.1016/j.jaerosci.2011.06.010.

Reagan, J. A., L. W. Thomason, B. M. Herman, and J. M. Palmer (1986), Assessment of atmospheric limitations on the determination of the solar spectral constant from ground-based spectroradiometer measurements, *IEEE Trans. Geosci. Remote Sens.*, *GE-24*, 258–266, doi:10.1109/TGRS.1986.289645.

Reichardt, J., U. Wandinger, M. Serwazi, and C. Weitkamp (1996), Combined Raman lidar for aerosol, ozone and moisture measurements, *Opt. Eng.*, *35*, 1457–1465, doi:10.1117/1.600681.

Rose, T., S. Crewell, U. Löhnert, and C. Simmer (2005), A network suitable microwave radiometer for operational monitoring of the cloudy atmosphere, *Atmos. Res.*, *75*, 183–200, doi:10.1016/j.atmosres.2004.12.005.

Sánchez, S. F., J. Aceituno, U. Thiele, D. Pérez-Ramírez, and J. Alves (2007), The night-sky at the Calar Alto observatory, *Publ. Astron. Soc. Pac.*, *119*, 1186–1200, doi:10.1086/522378.

Schmid, B., and C. Wehrli (1995), Comparison of sun photometer calibration by use of the Langley technique and the standard lamp, *Appl. Opt.*, *34*, 4500–4512, doi:10.1364/AO.34.004500.

Schmid, B., P. R. Spyak, S. F. Biggar, C. Wherli, J. Sekler, T. Ingold, C. Matzler, and N. Kampfer (1998), Evaluation of the applicability of solar and lamp radiometric calibrations of a precision sun photometer operating between 300 and 1025 nm, *Appl. Opt.*, *37*, 3923–3941, doi:10.1364/AO.37.003923.

Schmid, B., et al. (2001), Comparison of columnar water-vapor measurements from solar transmittance methods, *Appl. Opt.*, *40*, 1886–1895, doi:10.1364/AO.40.001886.

Smirnov, A., B. N. Holben, T. F. Eck, O. Dubovik, and I. Slutsker (2000), Cloud-screening and quality control algorithms for the AERONET database, *Remote Sens. Environ.*, *73*, 337–349, doi:10.1016/S0034-4257(00)00109-7.

Trenberth, K. E., et al. (2007), Observations: Surface and atmospheric climate change, in *Climate Change 2007: The Physical Science Basis: Working Group I Contribution to the Fourth Assessment Report of the Intergovernmental Panel on Climate Change*, edited by S. Solomon et al., chap. 3, pp. 235–336, Cambridge Univ. Press, New York.

Westwater, E. (1978), The accuracy of water vapor and cloud liquid determination by dual-frequency ground-based microwave radiometry, *Radio Sci.*, *13*, 667–685, doi:10.1029/RS013i004p00677.

Whiteman, D. N. (2003), Examination of the traditional Raman lidar technique. Part II. Evaluating the ratios for water vapor and aerosols, *Appl. Opt.*, *42*, 2593–2608, doi:10.1364/AO.42.002593.

Whiteman, D. N., S. H. Melfi, and R. A. Ferrare (1992), Raman lidar system for the measurement of water vapor and aerosols in the Earth's atmosphere, *Appl. Opt.*, *31*, 3068–3082, doi:10.1364/AO.31.003068.

Whiteman, D. N., et al. (2006), Raman lidar measurements during the International H_2O project. Part I: Instrumentation and analysis techniques, *J. Atmos. Oceanic Technol.*, *23*, 157–169, doi:10.1175/JTECH1838.1.

L. Alados-Arboledas, J. Fernández-Gálvez, H. Lyamani, F. Navas-Guzmán, F. J. Olmo, and D. Pérez-Ramírez, Departamento de Física Aplicada, Universidad de Granada, Campus de Fuentenueva s/n, E-18071 Granada, Spain. (dperez@ugr.es)